WARSAW UNIVERSITY OF TECHNOLOGY Index 351733
FACULTY OF CIVIL ENGINEERING
COMMITTEE FOR CIVIL AND WATER ENGINEERING
POLISH ACADEMY OF SCIENCES ISSN 1230-2945
DOI: 10.24425/ace.2024.149872
ARCHIVES OF CIVIL ENGINEERING
Vol. LXX ISSUE 2 2024
pp. 417 –430

Research paper

Stability analysis of ultra-high and steep reinforced soil fills slopes based on strength reduction

Yucong Gao[1], Yue Zhao[2], Tianyuan Xu[3], Jinlong Xu[4]

Abstract: The research focuses on solving the important problem of slope stability in the field of civil engineering. The study adopted an advanced strength double reduction coefficient method for slope stability analysis, which considers the different influence weights of cohesion and internal friction angle, and reduces them with different reduction coefficients to describe the stability of the slope. The simulation experiment results indicate that the attenuation degree of cohesion and internal friction angle affects slope stability. When the reduction coefficient of cohesion increases to 1.737 and the reduction coefficient of internal friction angle increases to 1.201, the slope is prone to instability and failure, and the safety factor of the calculated result is 1.493. Moreover, when the anti-slip pile is set in the middle of the slope (1/2), and the slope is in a critical state, the bending moment and shear force suffered by the anti-slip pile are both maximum, so the reinforcement effect is also the best.

Keywords: double reduction, reinforced soil, slope, stability, strength reduction, ultra high and steep

[1]Ph.D., School of Civil Engineering and Architecture, Northeast Electric Power University, Jilin 132012, China, e-mail: gyc19882023@163.com, ORCID: 0009-0000-8490-2981
[2]MSc., Xuzhou Power Supply Company, Xuzhou 221000, China, e-mail: jiushiwo5621@126.com, ORCID: 0009-0008-8290-4156
[3]MSc., State Grid Henan Electric Power Company, Zhengzhou 450000, China, e-mail: 13623855861@163.com, ORCID: 0009-0003-5783-708X
[4]MSc., State Grid Dongying Power Supply Company, Dongying 257100, China, e-mail: xujinlong3710@163.com, ORCID: 0009-0004-6364-7167

1. Introduction

In recent years, ultra-high and steep reinforced soil fill slopes have been widely used in railway, highway, dam, and other foundation projects [1, 2]. However, due to its special structure and reduced soil strength, there is significant uncertainty and safety hazards in the stability of the slope. Although researchers have conducted in-depth research on the calculation model, method, and parameters of the strength reduction method, there has not been sufficient and systematic research on the stability of ultra-high and steep reinforced soil fill slopes [3, 4]. When the shear stress in the slope rock and soil exceeds the shear strength of the soil, shear failure occurs [5, 6]. Due to the complexity of the geological environment and engineering conditions, the stability analysis of ultra-high and steep reinforced soil fill slopes is extremely cumbersome and complex [7]. Therefore, stability analysis based on strength reduction has very important engineering practical significance and theoretical research value for ultra-high and steep reinforced soil fill slopes [8, 9]. Studying the dual strength reduction method for the stability of ultra-high and steep reinforced soil fill slopes is innovative and has important theoretical significance and guiding value for enhancing the safety and stability of slopes.

2. Related work

Naeij et al. proposed a new method that defines the onset of instability through kinetic energy mutations and calculates the minimum safety factor based on the explicit finite element method. The calculation results of the method are consistent and do not require the assumption of a critical sliding surface, which is suitable for engineering under different conditions [10]. Sun et al. proposed a set of charts to evaluate the stability of rock slopes under various seismic loading conditions that meet the Hoek Brown criterion. The safety factor obtained through this chart is consistent with other methods [11]. Sysala et al. proposed an improved shear strength reduction method (MSSR) and its optimized variant (OPT-MSSR). The feasibility of the method was verified through two slope stability problems [12]. Bouzid calculated the dynamic response of the Caofeidian submarine slope during a similar Tangshan earthquake, and quantitatively reflected the impact of the earthquake on the slope through displacement values [13]. Wen et al. proposed a new rock contour establishment algorithm that considers the interlocking effect between rocks. The results showed that the N value increased with the increase of rock content [14].

Hong et al. conducted stability analysis on the artificial steep slope at the tunnel exit and evaluated the effectiveness of four reinforcement schemes [15]. Chen W et al. used the strength reduction method embedded with different unit codes to analyze the stability of a coal mine slope that underwent two rounds of reinforcement, and verified the instability of the slope during the initial reinforcement stage [16]. Lopez-Vinielles et al. proposed a method that combines digital photogrammetry, satellite radar interferometry, and geomechanical modeling for remote analysis of slope instability in open-pit mining areas [17]. Que et al. proposed a dimensionality reduction slope stability analysis method

(DR-SSAM), which considers the spatial effects of double V-shaped gully embankments. The rationality and effectiveness of this method in engineering applications were verified through case studies [18]. Yang et al. used digital image processing (DIP) technology to establish a real three-dimensional slope stability analysis slope structure model, and studied its stability using the latest strength reduction numerical manifold method (SRNMM) [19].

The finite element analysis method can be applied to different engineering environments, but the finite element strength reduction method also has some shortcomings. Therefore, a strength double reduction coefficient method is proposed to consider the weight effects of cohesion and internal friction angle. By reducing the cohesion and internal friction angle with different reduction coefficients, the stability of ultra-high and steep reinforced soil fill slopes is analyzed.

3. Application of strength double reduction in stability analysis of ultra-high and steep reinforced soil fills slopes

Slope stability is an important issue in civil engineering. When studying the numerical simulation of slope stability, it is necessary to consider the influence of soil constitutive model parameters on the calculation results.

3.1. Influencing factors analysis on the stability of ultra-high and steep reinforced soil fills slopes

In slope stability analysis, the SR method can maximize the stability of the slope. Unified standards have been established to determine whether the slope has reached the maximum stable state to make accurate evaluations in practical engineering [20]. The commonly used homogeneous slope is used to analyze the influence of slope shape and size, with a safety factor of 1.0. The model is shown in Fig. 1.

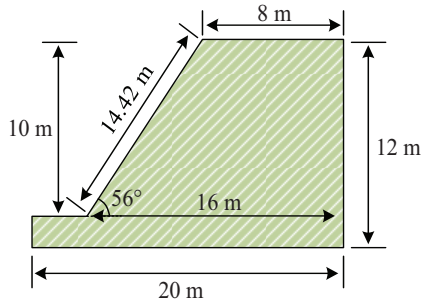

Fig. 1. Model diagram

In slope analysis, the stability of slopes under different slope ratios is studied. The height of the fixed slope is 10 m while maintaining the same IFA and cohesion. By changing the slope height ratio, i.e. the slope angle of the slope, the stability of the slope under different

slope height ratios is studied. In the model, the top edge length was adjusted to 8 m, 6 m, 4 m, 2 m, thereby reducing the slope ratio. The safety factors of slopes under different top edge lengths are displayed in Table 1.

Table 1. Slope Factor of safety under different top side length

Top edge length (m)	Safety factor	
	FC1	FU1
8	1.06	0.99
6	1.18	1.09
4	1.18	1.14
2	1.28	1.31

Table 1 shows that the slope has undergone slope changes, but its stability has not shown a straight downward trend. Meanwhile, this also indicates that the steeper the slope, the more unstable its stability is.

The cohesive force was sequentially increased by 5 kPa, resulting in slope models with cohesive forces of 7.38 kPa, 12.38 kPa, 17.38 kPa, and 22.38 kPa, respectively. The safety factors under different elastic moduli and cohesive forces are calculated. Table 2 displays the results.

Table 2. SFs under different elastic moduli and cohesive force

E (MPa)	Safety factor		Cohesive force (kPa)	Safety factor	
	FC1	FU1		FC1	FU1
100	1.06	0.99	7.38	0.79	0.77
80	1.06	0.99	12.38	1.06	0.99
60	1.06	0.99	17.38	1.22	1.18
40	1.06	0.99	22.35	1.42	1.38
20	1.06	0.99	27.38	1.58	1.52

In Table 2, the elastic modulus has a small impact on the stability of the slope. The slope safety coefficient calculated under different elastic moduli is consistent. Therefore, when analyzing the slope stability, the impact on slope stability can be ignored.

3.2. The field boundary quantity in slope stability strength reduction method

The numerical calculation tool used in the study is ABAQUS analysis software, which is a large finite element program system. In slope stability analysis, the SF is applied as an indicator to evaluate the slope stability. The expression for the SF is shown in Eq. (3.1).

$$F_s^i = M_f^i / M^i (i = 1, 2, \ldots, n) \tag{3.1}$$

In Eq. (3.1), F_s^i is the SF of the i-th sliding surface. M_f^i is the maximum anti-slip moment provided by the soil below the i-th assumed sliding surface to the sliding body. M_f^i is the sliding moment generated by the sliding body above the i-th assumed sliding surface. The minimum value between the three is selected and defined as $F_s^i = \min\left(F_s^i\right)$. The minimum is the SF of the slope.

Usually, the SF of a slope is between 1.0 and 10.0 [21]. To convert the temperature field into a shear strength parameter of the slope, it is assumed that the temperature field variable θ increases from 0 to 100. The cohesion force c and IFA φ decrease with the temperature field until they reach $0.1c$ and $0.1\tan\varphi$. The elastic modulus $1/F_s$ is reduced from 1.0 to 0.1. The mathematical relationship is shown in Eq. (3.2).

$$\frac{c}{c_1} = \frac{\tan\varphi}{\tan\varphi_1} = \frac{1}{F_s} = 1 - \frac{\theta}{100} \times 0.9 \tag{3.2}$$

In Eq. (3.2), c_1 and $\tan\varphi_1$ represent the cohesion and internal friction angle during the reduction process, respectively. When the time step t increases from 0 to 10, the temperature field θ is defined as linearly increasing to 100. Therefore, the Eq. (3.3) can be obtained.

$$\theta = 100t \tag{3.3}$$

The relationship between safety factor and time step can be obtained by combining Eqs. (3.2) and (3.3), as shown in Eq. (3.4).

$$F_s = \frac{1}{1 - 0.9t} \tag{3.4}$$

Similarly, the relationship between the two can be obtained when the safety factor is less than 1.0, as shown in Eq. (3.5).

$$F_s = \frac{1}{f} = \frac{1}{g - ht} \tag{3.5}$$

In Eq. (3.5), f is a linear field variable, g is the initial value of the field variable, h is the change value of the field variable. According to the meaning of the reduction coefficient, F_s should be greater than 0. In ABAQUS FEA software, the value range of time step t is [0,1]. The values of g and h should be positive, while g/h is not 0. The g affects the minimum value of the reduction coefficient. The $g \cdot h$ may affect the maximum value of the reduction coefficient. In the above derivation, when g is taken as 1.0 and h is taken as 0.9, the value range of F_s is [1, 10]. Therefore, flexible values should be taken based on the actual slope conditions. The process of strength reduction method in ABAQUS software is shown in Fig. 2.

Firstly, establish a model, set material properties, and assemble components. Then, set up the analysis steps and add interactions. Then set boundary conditions, load effects, and grid division. Finally, submit the task for calculation.

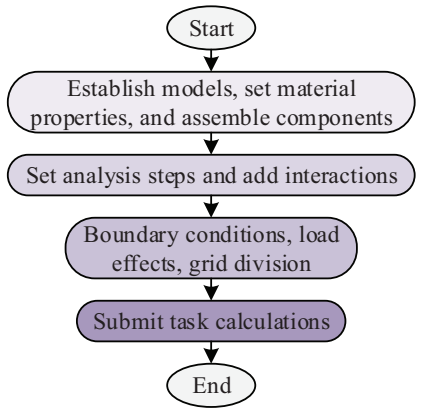

Fig. 2. Software calculation process

3.3. Stability analysis of ultra-high and steep reinforced soil fills slopes based on the strength double reduction coefficient method

The traditional SR uses the same RC to reduce the cohesion and IFA. The reduction factor when the slope reaches a critical state is the SF of the slope. The reduction method for this single RC is defined as proportional reduction. The strength reserve area is used to define the safety factor. Fig. 3 displays the strength reserve concept.

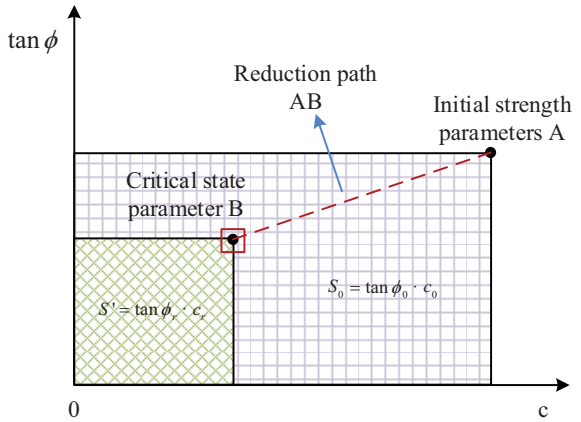

Fig. 3. Schematic diagram of strength reserve concept

In Fig. 3, the coordinate product of point A is considered as the strength reserve area of the initial state of the slope. The safety factor of a slope is the ratio of the true shear capacity of the soil to the critical shear capacity at failure, as expressed in Eq. (3.6).

(3.6) $$F_s = \frac{c_0}{c'} = \frac{\tan\varphi_0}{\tan\varphi'}$$

In Eq. (3.6), c_0 and φ_0 are the actual shear capacity parameters of the soil, namely the initial cohesion and initial IFA. c' and φ' are the shear strength parameters when the soil reaches a critical equilibrium state, which are the reduced cohesion and IFA. The focus of the SR method is to ratio the cohesion forces c and $\tan\varphi$ to the reduction coefficient F_s. Two new soil strength parameters c' and $\tan\varphi'$ are obtained. Then two sets of soil shear strength parameters are inputted into the original formula again for calculation. This process is repeated until the slope is in the ultimate equilibrium state, and then loses stability and fails. The most dangerous sliding surface of the slope was analyzed. The reduction coefficient F_s corresponding to this sliding surface is the minimum SF of the entire slope. The expression is displayed in Eq. (3.7).

$$\begin{cases} c' = \frac{c_0}{F_s} \\ \varphi' = \arctan(\frac{\tan\varphi_0}{F_s}) \end{cases} \tag{3.7}$$

When using ABAQUS to analyze slope stability problems, material parameters can change with changes in field variables. The relationship between shear strength and field variables is shown in Eq. (3.8).

$$\begin{cases} c = c_0/F(f_1) \\ \tan\varphi = \tan\varphi_0/F(f_2) \end{cases} \tag{3.8}$$

In Eq. (3.8), f_1 is the field variable of cohesion. f_2 is the field variable of the tangent value of the internal friction angle. $F(f_1)$ and $F(f_2)$ are the RCs for the variation of cohesion and internal friction angle with changes in field variables, respectively. The two intervals are set as $[a, b]$ and $[d, e]$. a, b, d, and e are constants. The values of shear strength parameters during finite element calculation are shown in Eq. (3.9).

$$\begin{cases} \frac{c_0}{b} \le c \le \frac{c_0}{a} \\ \frac{\tan\varphi_0}{e} \le \tan\varphi \le \frac{\tan\varphi_0}{d} \end{cases} \tag{3.9}$$

The relationship between the RC and the shear strength parameters is shown in Eq. (3.10).

$$\begin{cases} F_1 = c_0/c \\ F_2 = \tan\varphi_0/\tan\varphi \end{cases} \tag{3.10}$$

In Eq. (3.10), F_1 and F_2 are the RCs of cohesion and IFA. The relationship between the RC and the shear strength parameters are shown in Eq. (3.11).

$$\begin{cases} F_1 = F(f_1) \\ F_2 = F(f_2) \end{cases} \tag{3.11}$$

Assuming that the time step t in ABAQUS increases from g to h. The functions $F(f_1)$ and $F(f_2)$ linearly monotonically increase within the interval. Therefore, when calculating the time step t_1 without convergence, the relationship between the RC and the time step is shown in Eq. (3.12).

$$\begin{cases} \frac{t_1 - g}{h - t_1} = \frac{F_1 - a}{b - F_1} \\ \frac{t_1 - g}{h - t_1} = \frac{F_2 - c}{d - F_2} \end{cases} \tag{3.12}$$

After calculating Eq. (3.12), Eq. (3.13) can be obtained.

$$\begin{cases} F_1 = \dfrac{a(h-t_1)+b(t_1-g)}{h-g} \\ F_2 = \dfrac{d(h-t_1)+e(t_1-g)}{h-g} \end{cases} \tag{3.13}$$

In the strength double RC method, the combination of F_1 and F_2 is influenced by various influencing factors, resulting in many possible combinations. To simplify the calculation, the cohesion and IFA can be set as a proportional relationship, i.e. $F_1 = kF_2$. Through analysis, the coefficients a, b, d and e are all included in the range of reduction coefficients. When the reduction coefficient varies within the range of 0.5–2.0, $a = 0.5$ and $b = 2$. Therefore, $d = 0.5/k$, $e = 2/k$. In ABAQUS, when the time step gradually increases from the initial $g = 0$ to $h = 1$, Eq. (3.14) can be obtained.

$$\begin{cases} F_1 = \dfrac{3}{2}t_1 + \dfrac{1}{2} \\ F_2 = \dfrac{1}{k}\left(\dfrac{3}{2}t_1 + \dfrac{1}{2}\right) \end{cases} \tag{3.14}$$

To implement the strength double reduction coefficient method in ABAQUS, two field variables can be introduced. To simplify the calculation and verify the feasibility in engineering, assumptions are made on the reduction ratio of cohesion and IFA in the strength double RC method. By analyzing the variation of the reduction coefficient with displacement, the curves of the cohesion and IFA RC with displacement can be established, as shown in Fig. 4.

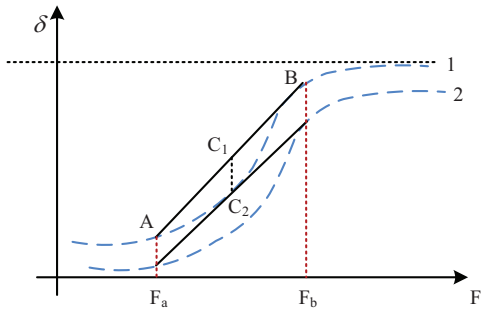

Fig. 4. Curve of cohesion and IFA reduction coefficient with displacement

In Fig. 4, dashed line 1 represents the relationship between the RC of cohesion and displacement. The dashed line 2 represents the relationship between the RC of internal friction angle and displacement. C1 and C2 are the midpoints of dashed lines 1 and 2. It reflects the cohesion and IFA at the middle position of the line connecting the maximum and minimum reduction coefficients. Dash 1 and Dash 2 are established using the scale factor k. Therefore, there is a proportional relationship of k between line 1 and line 2, that is, Cl/C2 = k.

4. Application analysis of stability for ultra-high and steep reinforced soil fills slopes based on strength reduction

4.1. Stability analysis of ultra-high and steep reinforced soil fill slopes based on strength reduction

The selected site for the research experiment is a certain oil transportation station, which is located on a loess beam slope and presents a stepped and gently inclined shape. The safety level of this slope is Level 1, and a safety factor of not less than 1.35 is required. The study adopts a combination of reinforced soil slopes and reinforced soil retaining walls for design. The specific design scheme cross-section is shown in Fig. 5.

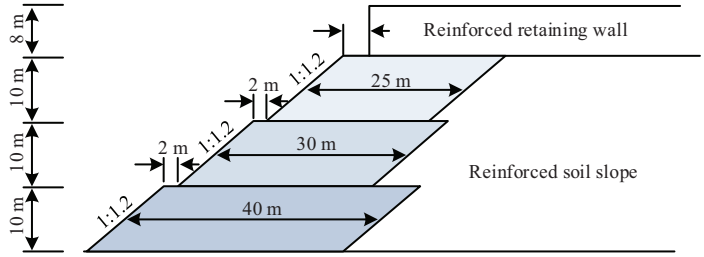

Fig. 5. Specific design plan section

It is important to consider the filtration characteristics when analyzing the stability of ultra-high and steep reinforced soil fill slopes. The filtration characteristics mainly refer to the water flow filtration characteristics and particle separation phenomenon between filled and reinforced soil. The consideration of filtration characteristics can affect the drainage performance, impermeability performance, and overall stability of filled and reinforced soil. For better analysis, it is assumed that there is a proportional relationship between the cohesion RC and the IFA reduction coefficient, i.e. $k = F_1/F_2$. Different k values are analyzed. The results are shown in Fig. 6.

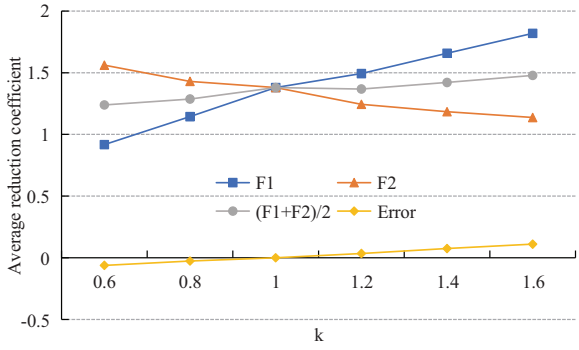

Fig. 6. The relationship between average reduction coefficient and k

In Fig. 6, when the value of k is 0.8, the average reduction coefficient is 1.287, which is slightly smaller than the SF obtained by the traditional single reduction method.

In the dynamic calculation of slopes, only horizontal seismic forces are considered. The horizontal recorded value of the Koyna earthquake in India is selected as the seismic wave interception. A horizontal seismic acceleration of 0.02 g is applied. The action time is 10 s. Fig. 7 is the horizontal seismic waves.

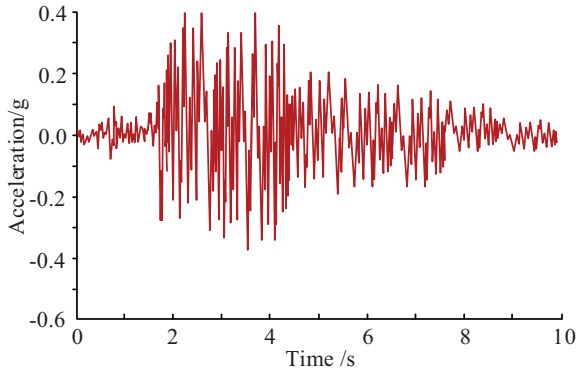

Fig. 7. Schematic diagram of horizontal Seismic wave

Through analysis, the failure of slopes under earthquake action is a dynamic and continuous process, rather than occurring immediately at a certain moment. Some important information can be obtained from the simulation results. The failure mechanism of slopes under earthquake action is not all shear failure, but includes the failure generated on the slope surface and top.

4.2. Analysis of the impact of anti slip piles on safety factors

For this three-dimensional slope, anti-slip piles with a diameter of 0.8m are used for reinforcement, with a spacing of $D/d = 6$. The elastic modulus of the anti-slip piles is $E = 25$ GPa. The ratio of the anti-slip piles to the slope angle position is $L_x/L = 1/2$. The geometric schematic diagram of anti slip pile reinforcement slope is shown in Fig. 8.

The strength double reduction coefficient method is applied to analyze the stability of the three-dimensional slope reinforced by the anti-slip pile. The relationship curve between the horizontal displacement (HD) of the slope top and the RC is shown in Fig. 9.

In Fig. 9, as the reduction process progresses, when the RC of cohesion increases to 1.737 and the reduction coefficient of internal friction angle increases to 1.201, there is a turning point in the HD at the top of the slope. Therefore, according to the definition of comprehensive SF, the SF of the slope is 1.493.

The proportion of the distance between the anti-slip pile and the slope angle position selected in the study is $L_x/L = 0$, 1/6, 1/3, 1/2, 2/3, 5/6, and 1. Based on this condition, the strength double RC method is used to analyze the slope after reinforcement by anti-slip piles. Fig. 10 shows the effect of the location of anti-slip piles on the safety factor of the slope.

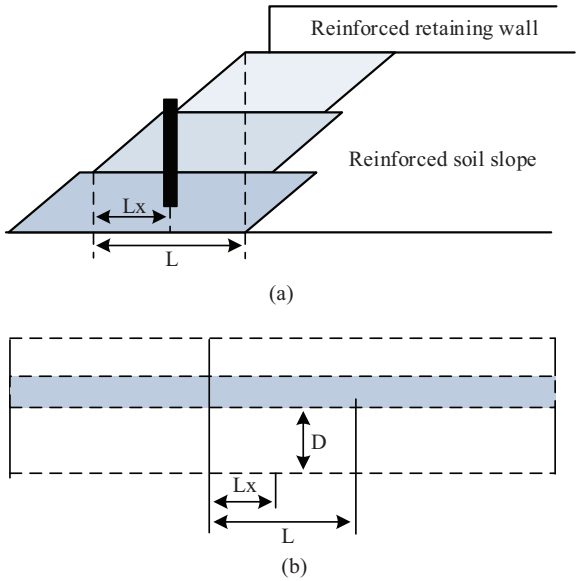

Fig. 8. Geometric schematic diagram of slope reinforcement with anti slip piles: a) Cross section of anti slip pile reinforcement slope, b) Layout plan of anti slip pile reinforcement slope

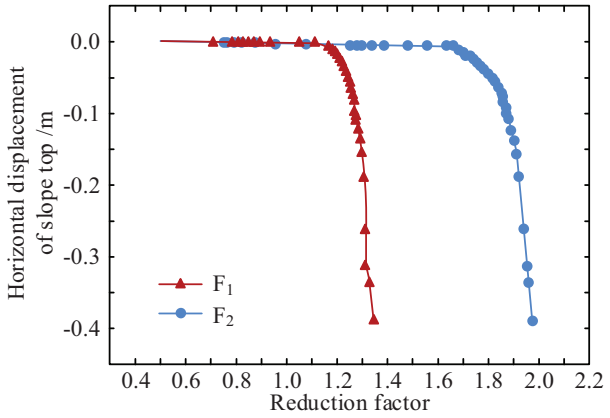

Fig. 9. Relationship curve between HD of slope top and RC

In Fig. 10, as the position L_x/L of the anti-slip pile gradually increases, the SF of the slope first increases and then decreases. According to the trend of safety factor changes, when the position L_x/L of the anti-skid pile is between 1/3 and 1/2, the anti-skid pile has the greatest obstruction effect on the landslide mass. The reinforcement effect is also more ideal.

For different locations of anti-slip piles, when critical sliding occurs on the slope, the deflection, bending moment, and shear force changes in the X-direction of the pile body are shown in Fig. 11.

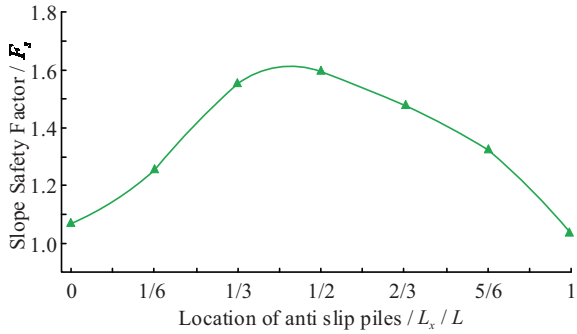

Fig. 10. Influence of anti-slide pile position on slope factor of safety

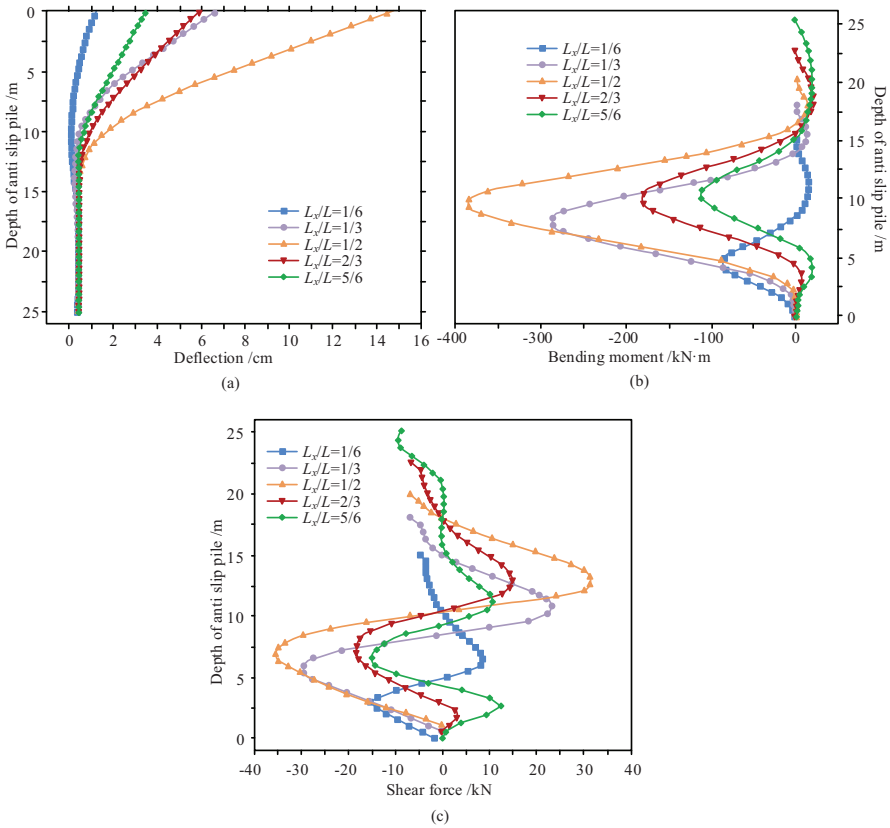

Fig. 11. The influence of the position of anti-slip piles on pile deflection, bending moment, and shear force: a) The influence of anti-skid pile position on pile deflection, b) The influence of anti-skid pile position on pile bending moment, c) The influence of anti-skid pile position on pile shear force

According to Fig. 11, when the anti-slip pile is ($L_x/L = 1/2$), the maximum deflection of the corresponding pile body occurs when the slope undergoes critical sliding. At this point, the safety factor is also the highest. When set at $L_x/L = 1/3$ and 2/3, the deflection of the pile body is equivalent when the slope undergoes critical sliding. When the slope at $L_x/L = 1/6$ and 5/6 experiences critical sliding, the deflection of the pile is relatively small. When the anti-slip pile is set in the middle of the slope ($L_x/L = 1/2$), and the slope is in a critical state, the bending moment and shear force suffered by the anti-slip pile are both maximum. Therefore, the reinforcement effect is also better.

5. Conclusions

Regarding the impact of slope stability and the evaluation of reinforcement effectiveness, the strength double RC method is applied for slope stability analysis. Meanwhile, in practical work, the anti-slip pile reinforcement method is applied to effectively improve the stability of the slope. In the beginning of strength reduction, the HD at the top of the slope remains almost unchanged. When the RC of cohesion increases to 1.737, and the reduction coefficient of internal friction angle increases to 1.201, a turning point occurs in the HD of the top of the slope. At this point, the slope undergoes instability and failure, and the comprehensive safety coefficient of the slope is 1.493. Furthermore, the location of anti-slip piles has great impacts on the slope stability. When the position of the anti-slip pile is between 1/3 and 1/2, the slope has the maximum safety reserve. The corresponding slope safety factor is the highest. The research results indicate that the strength double reduction coefficient method has good applicability in slope stability analysis. However, due to the lack of practical engineering experience in research, there are still many issues that need to be further addressed. Firstly, the current method applies the nonlinear proportion of the reduction coefficient as the field variable changes. You can consider using programming to achieve improvements. Secondly, for the calculation of the safety factor, the average value of the results using the characteristic point displacement criterion and the plastic zone criterion is also open to discussion. Therefore, determining a quantitative instability criterion for analyzing slope safety factors is a very meaningful research direction.

References

[1] M. Jia, W. Zhu, and C. Xu, “Performance of a 33 m high geogrid reinforced soil embankment without concrete panel”, *Geotextiles and Geomembranes*, vol. 49, no. 1, pp. 122–129, 2021, doi: 10.1016/j.geotexmem.2020.07.008.

[2] X. Zhou, H. Jiang, M. Zhou, and Y. Hu, “Case study: Extension of MSW landfill with reinforced earth berm”, *Waste Management*, vol. 164, pp. 37–46, 2023, doi: 10.1016/j.wasman.2023.03.024.

[3] Y. Fang, B. Luo, T. Zhao, D. He, B. Jiang, and Q. Liu, “ST-SIGMA: Spatio-temporal semantics and interaction graph aggregation for multi-agent perception and trajectory forecasting”, *CAAI Transactions on Intelligence Technology*, vol. 7, no. 4, pp. 744–757, 2022, doi: 10.1049/cit2.12145.

[4] W.H. Yuan, K. Liu, W. Zhang, B. Dai, and Y. Wang, “Dynamic modeling of large deformation slope failure using smoothed particle finite element method”, *Landslides*, vol. 17, pp. 1591–1603, 2020, doi: 10.1007/s10346-020-01375-w.

[5] Z. Tao, Y. Shu, X. Yang, Y. Peng, C. Qiang, and H. Zhang, "Physical model test study on shear strength characteristics of slope sliding surface in Nanfen open-pit mine", *International Journal of Mining Science and Technology*, vol. 30, no. 3, pp. 421–429, 2020, doi: 10.1016/j.ijmst.2020.05.006.

[6] A. Morcioni, T. Apuani, and F. Cecinato, "The role of temperature in the stress–strain evolution of Alpine rock-slopes: Thermo-mechanical modelling of the Cimaganda rockslide", *Rock Mechanics and Rock Engineering*, vol. 55, no. 4, pp. 2149–2172, 2022, doi: 10.1007/s00603-022-02786-y.

[7] J. Wei, Y. Wei, and X. Huang, "A meso-scale study of the influence of particle shape on shear deformation of coarse-grained soil", *Hydrogeology & Engineering Geology*, vol. 48, no. 1, pp. 114–122, 2021, doi: 10.16030/j.cnki.issn.1000-3665.202002017.

[8] Y. Xiong, B. Fang, J. Zhang, K. Yan, and Y. Zhu, "Subsurface stresses analysis of flexible ball bearing with bendable races in a harmonic reducer by superimposition method", *Proceedings of the Institution of Mechanical Engineers, Part J: Journal of Engineering Tribology*, vol. 236, no. 6, pp. 1244–1259, 2022, doi: 10.1177/13506501211049957.

[9] M. Barma and U. M. Modibbo, "Multiobjective mathematical optimization model for municipal solid waste management with economic analysis of reuse/recycling recovered waste materials", *Journal of Computational and Cognitive Engineering*, vol. 1, no. 3, pp. 122–137, 2022, doi: 10.47852/bonviewJCCE149145.

[10] M. Naeij, H. Ghasemi, D. Ghafarian, and Y. Javanmardi, "Explicit finite element analysis of slope stability by strength reduction", *Geomechanics and Engineering*, vol. 26, no. 2, pp. 133–146, 2021, doi: 10.12989/gae.2021.26.2.133.

[11] C. Sun, J. Chai, T. Luo, Z. Xu, Y. Qin, X. Yuan, and B. Ma, "Stability charts for pseudostatic stability analysis of rock slopes using the nonlinear Hoek–Brown strength reduction technique", *Advances in Civil Engineering*, vol. 2020, no. 3, pp. 1–16, 2020, doi: 10.1155/2020/8841090.

[12] S. Sysala, E. Hrubesova, Z. Michalec, and F. Tschuchnigg, "Optimization and variational principles for the shear strength reduction method", *International Journal for Numerical and Analytical Methods in Geomechanics*, vol. 45, no. 16, pp. 2388–2407, 2021, doi: 10.1002/nag.3270.

[13] D.A. Bouzid, "Finite element analysis of a slope stability by incrementally increasing the mobilised principal stress deviator", *Geomechanics and Geoengineering*, vol. 17, no. 5, pp. 1554–1574, 2022, doi: 10.1080/17486025.2021.1955157.

[14] H. Wen, Z. Yao, W. Hui, Z. Zhao, and P. Jiang, "Soil-Rock slope stability analysis under top loading considering the nonuniformity of rocks", *Advances in Civil Engineering*, vol. 2020, art. no. 9575307, 2020, doi: 10.1155/2020/9575307.

[15] Y. Hong, Z. Shao, G. Shi, and J. Liu, "Stability and countermeasures for a deposit slope with artificial scarp: Numerical analysis and field monitoring", *Advances in Civil Engineering*, vol. 2020, art. no. 8822080, 2020, doi: 10.1155/2020/8822080.

[16] W. Chen, D. Li, T. Ma, H. Fu, and Y. Du, "Stability analysis of a slope considering two reinforcement processes", *Geofluids*, vol. 2020, art. no. 8828747, 2020, doi: 10.1155/2020/8828747.

[17] J. Lopez-Vinielles, P. Ezquerro, J. A. Fernandez-Merodo, et al., "Remote analysis of an open-pit slope failure: Las Cruces case study, Spain", *Landslides*, vol. 17, pp. 2173–2188, 2020, doi: 10.1007/s10346-020-01413-7.

[18] Y. Que, X. Chen, Y. Chen, Z. Jiang, Y. Qiu, and S. Easa, "Stability analysis of double V-shaped gully embankment: A dimension-reduced calculation method", *Canadian Journal of Civil Engineering*, vol. 49, no. 1, pp. 52–63, 2022, doi: 10.1139/cjce-2019-0783.

[19] Y. Yang, T. Chen, W. Wu, and H. Zheng, "Modelling the stability of a soil-rock-mixture slope based on the digital image technology and strength reduction numerical manifold method", *Engineering Analysis with Boundary Elements*, vol. 126, pp. 45–54, 2021, doi: 10.1016/j.enganabound.2021.02.008.

[20] D. Mrówczyński, T. Gajewski, and T. Garbowski, "Application of the generalized nonlinear constitutive law in 2D shear flexible beam structures", *Archives of Civil Engineering,* vol. 67, no. 3, pp. 157–176, 2021, doi: 10.24425/ace.2021.138049.

[21] S. Lin, H. Zheng, W. Jiang, W. Li, and G. Sun, "Investigation of the excavation of stony soil slopes using the virtual element method", *Engineering Analysis with Boundary Elements*, vol. 121, no. 3, pp. 76–90, 2020, doi: 10.1016/j.enganabound.2020.09.005.

Received: 2023-09-04, Revised: 2023-11-21